Nature Communications

https://doi.org/10.1038/s41467-026-69070-3

Article in Press

Bell correlations between momentum-entangled pairs of $^4He^*$ atoms

Received: 29 April 2025

Accepted: 19 January 2026

Cite this article as: Athreya, Y.S., Kannan, S., Yan, X.T. *et al.* Bell correlations between momentum-entangled pairs of $^4He^*$ atoms. *Nat Commun* (2026). https://doi.org/10.1038/s41467-026-69070-3

Y. S. Athreya, S. Kannan, X. T. Yan, R. J. Lewis-Swan, K. V. Kheruntsyan, A. G. Truscott & S. S. Hodgman

Bell correlations between momentum-entangled pairs of ^{4}He* atoms

Y. S. Athreya,[1] S. Kannan,[1] X. T. Yan,[1] R. J. Lewis-Swan,[2,3]
K. V. Kheruntsyan,[4] A. G. Truscott,[1] and S. S. Hodgman[1,*]

[1] *Research School of Physics, Australian National University, Canberra 2601, Australia*
[2] *Homer L. Dodge Department of Physics and Astronomy, The University of Oklahoma, Norman, Oklahoma 73019, USA*
[3] *Center for Quantum Research and Technology, The University of Oklahoma, Norman, Oklahoma 73019, USA*
[4] *School of Mathematics and Physics, University of Queensland, Brisbane, Queensland 4072, Australia*

(Dated: January 11, 2026)

Nonlocal entanglement between pair-correlated particles is a highly counter-intuitive aspect of quantum mechanics, where measurement on one particle can instantly affect the other, regardless of distance. While the rigorous Bell's inequality framework has enabled the demonstration of such entanglement in photons and atomic internal states, no experiment has yet involved motional states of massive particles. Here we report the experimental observation of Bell correlations in motional states of momentum-entangled ultracold helium atoms. Momentum-entangled pairs are first generated via s-wave collisions. Using a Rarity-Tapster interferometer and a Bell-test framework, we observe atom-atom correlations required for violation of a Bell inequality. This result shows the potential of ultracold atoms for fundamental tests of quantum mechanics and opens new avenues to studying gravitational effects in quantum states.

INTRODUCTION

Bell's inequality serves as a fundamental test for distinguishing between classical local realism and the nonlocal correlations predicted by quantum mechanics [1, 2]. Its violation is a cornerstone of quantum mechanics, directly challenging local hidden variable (LHV) theories and demonstrating the nonlocal nature of quantum entangled states. Such violations of Bell's inequality have been experimentally observed in various systems, predominantly focusing on *internal* degrees of freedom such as the polarization states of massless photons [3–6] and atomic spin states [7–11]. These Bell tests involve measuring so-called Bell correlations – a set of certain joint probability measurements on a pair of particles – that provide compelling evidence supporting the nonlocal nature of quantum entanglement.

Extending Bell tests to *external*, motional degrees of freedom – particularly momentum-entanglement – of massive particles offers a deeper understanding of quantum nonlocality and its implications for the foundations of quantum mechanics. Momentum-entangled states of massive particles, for instance, enable fundamental experiments involving couplings to gravitational fields, thereby enabling tests of theories that seek to reconcile the currently incompatible frameworks of quantum mechanics and general relativity [12–16]. However, experimental demonstrations of Bell inequality violations in motional states remain limited, with only photonic demonstrations to date [17].

Ultracold atomic systems, and particularly metastable helium (^{4}He*) atoms [18], have been proposed as promising systems for observing Bell nonlocality in momentum-entangled massive particle states [19]. The high internal energy of metastable helium enables precise single-atom detection with high spatial and temporal resolution. Efforts towards this goal so far [20–22] include demonstrating a matter-wave Rarity-Tapster configuration [17] interferometer using colliding Bose-Einstein Condensate (BECs) of ^{4}He* [23] and showing control over the relative phases of momentum modes in atomic Bragg diffraction [24]. Additionally, Perrier *et al.* [25] validated the quantum statistics of a two-mode squeezed vacuum state generated via atomic four-wave mixing in BEC collisions, either in free space [23, 26–29], within an optical lattice potential [22, 30–34] or via cavity mediated interaction [35]. In the low-mode occupancy limit, such states approximate the archetypal Bell state that maximally violates Bell's inequality. However, a demonstration of nonlocal behaviour in this system has remained elusive.

This work presents the first experimental observation of Bell correlations necessary to demonstrate nonlocality in momentum-entangled pairs of atoms. By colliding two BECs of ^{4}He*, we generate pairs of correlated atoms with opposite momenta via spontaneous s-wave scattering. We implement the matter-wave analog of the Rarity-Tapster interferometric scheme and measure phase-sensitive momentum correlations between scattered atoms after passing through separate interferometric arms. Analyzing these momentum correlations within the framework of a Bell inequality test, we observe strong correlations that provide direct evidence of the nonlocal quantum nature of the system and are unable to be explained by a large class of LHV theories.

RESULTS

Momentum-entanglement via BEC collision. Our experiment begins with a BEC of helium atoms mag-

* sean.hodgman@anu.edu.au

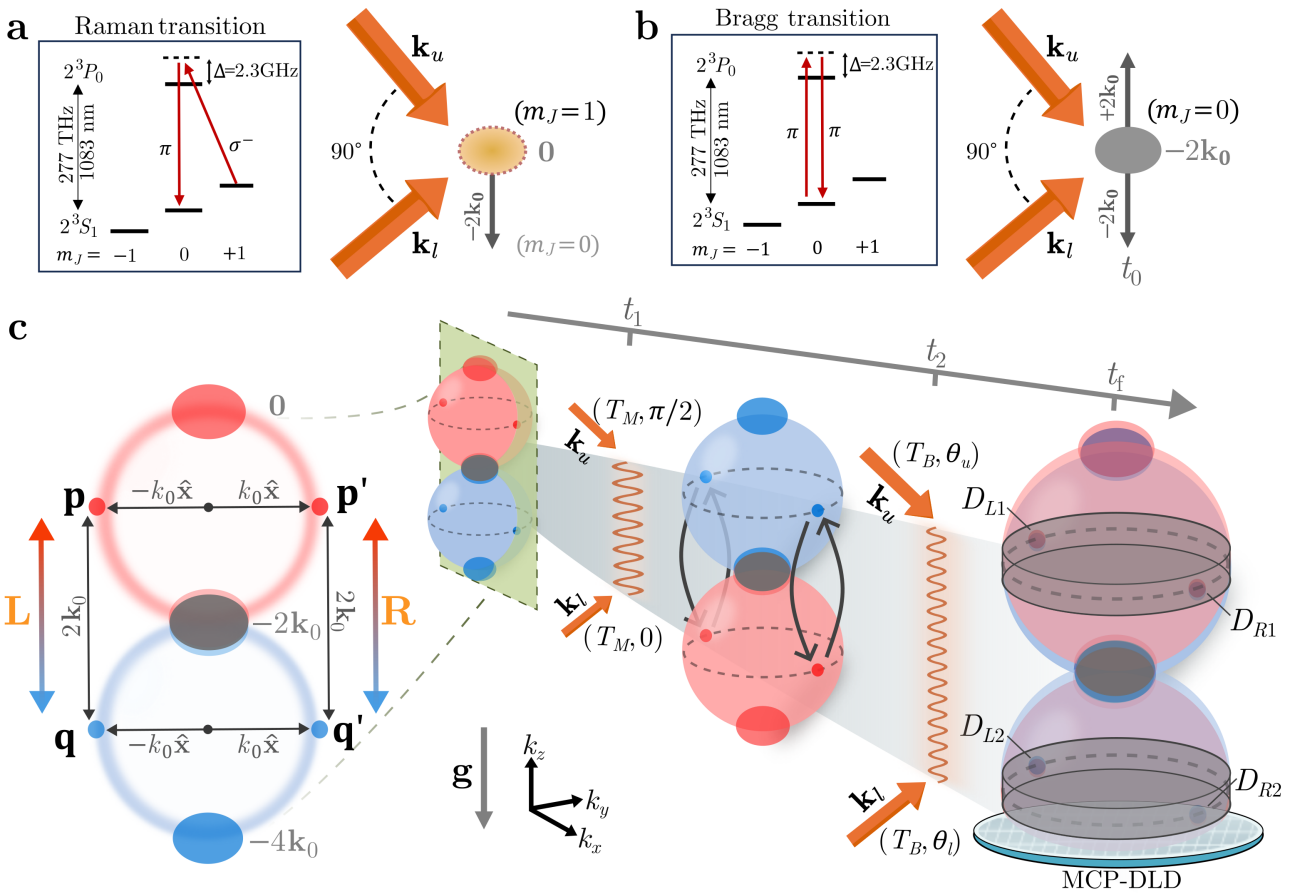

Fig. 1. Schematic of the experimental procedure in momentum space. **a** Orthogonal laser beams with wavevectors $\mathbf{k}_u$ and $\mathbf{k}_l$ (orange arrows) initially drive a two-photon Raman transition to transfer ^{4}He* atoms to the m_J=0 sublevel and impart momentum of $-2k_0\hat{\mathbf{z}}$ in the direction of gravity ($\mathbf{g}$). **b** A Bragg transition at t_0 coherently splits the atoms into momentum modes: $\mathbf{0}$,$-2\mathbf{k}_0$,$-4\mathbf{k}_0$. The $\mathbf{0}$ and $-2\mathbf{k}_0$ components (red) and $-2\mathbf{k}_0$ and $-4\mathbf{k}_0$ components (blue) collide to create two spherical s-wave scattering halos of entangled pairs of atoms. **c** A Rarity-Tapster interferometer mixes atom pairs in momentum modes $\{\mathbf{p},\mathbf{p}'\}$ and $\{\mathbf{q},\mathbf{q}'\}$ from each halo, which are entangled through momentum conservation. Bragg transition pulses couple the atoms in separate arms of the interferometer, denoted by L for $(\mathbf{p},\mathbf{q})$ and R for $(\mathbf{p}',\mathbf{q}')$. At t_1 and t_2, we apply mirror and beamsplitter pulses of duration T_M and T_B and impart phases $\pi/2$ and $\phi_{L,R}=\theta_u-\theta_l$, respectively, equal to the phase difference between the upper (θ_u) and lower (θ_l) Bragg beams. After a fall-time $t_f\approx 0.416$ s the scattered atoms are detected on a multichannel plate and delay line detector (MCP-DLD). Detection windows (grey-shaded annuli) centred around each halo's equatorial plane yield multi-particle correlations between $\{D_{L1},D_{L2},D_{R1},D_{R2}\}$ at the output of the interferometer.

netically trapped (see Methods section for details) in the $m_J=+1$ sub-level of the long-lived 2^3S_1 metastable state [18, 36]. Following trap switch-off, momentum-entanglement is created and manipulated via resonant two-photon Raman and Bragg transitions using two orthogonal off-resonant laser beams (see Methods section for details). Figure 1 shows a schematic representation of the experimental procedure.

We first transfer 90(5)% of the BEC atoms to the magnetically insensitive $m_J=0$ sub-level via a Raman pulse. This pulse also imparts a two-photon recoil momentum of $-2\hbar\mathbf{k}_0$ in the $\hat{z}$-direction, where $\mathbf{k}_0=k_0\hat{\mathbf{z}}$ and $k_0=K/\sqrt{2}$ based on our beam geometry. Here $K=2\pi/\lambda$ is the wavenumber of the laser beam and λ=1083.19 nm denotes the wavelength of the incident laser beams. By transferring atoms to a magnetically insensitive state, we prevent momentum distortions that may occur due to stray magnetic fields in the vacuum chamber during the experiment.

We then coherently split the condensate of $m_J=0$ atoms, already moving with momentum $-2\hbar\mathbf{k}_0$, by imparting $\pm2\hbar\mathbf{k}_0$ momentum to the atoms via a two-photon Bragg transition pulse [28, 37] (Fig. 1b). This 'collision pulse' splits the bulk of the condensate atoms into three momentum orders: $\mathbf{0}$, $-2\hbar\mathbf{k}_0$, $-4\hbar\mathbf{k}_0$. As the momentum displaced condensates spatially separate, pairs of constituent atoms undergo s-wave collisions [26], forming spherically symmetric halos of spontaneously scattered atom pairs in momentum space. Each halo is centred about the centre-of-mass (COM) momentum of the rel-

evant pair of colliding condensates. Since we split the condensate into three momentum orders, we observe the formation of two distinct scattering halos: one between **0** and $-2\hbar\mathbf{k}_0$ (red), and another between $-2\hbar\mathbf{k}_0$ and $-4\hbar\mathbf{k}_0$ (blue), as illustrated in Fig. 1c.

This collision process creates momentum-entangled atom pairs analogous to the process of four-wave mixing in quantum optics [26, 27], in which entangled photon pairs are generated through spontaneous parametric down-conversion [38]. In this context, each of the halos can be characterized as an ensemble of two-mode squeezed vacuum states, with atom pairs occupying diametrically opposite momentum modes within the halo, in accordance with conservation of momentum and energy [19, 23]. We operate our experiment in the low-gain regime with mode occupancies $\bar{n} \ll 1$, i.e., a low average number of atoms in a scattered momentum mode [39]. Under such conditions, we analyse data with a single pair detected in the relevant output momentum ports of the Rarity-Tapster interferometer, which allows us to truncate and transform the halo's mode-squeezed states into a prototypical Bell state for atoms [19, 23] (see Supplementary Note 1). The reduced and truncated initial state (i.e., the state of a quartet of scattering modes that form the initial state at the input ports of the interferometer) can be approximated to acquire the form of a prototypical Bell state [19, 23]:

$$|\Psi\rangle \approx \frac{1}{\sqrt{2}}(|1\rangle_{\mathbf{p}}|1\rangle_{\mathbf{p}'}|0\rangle_{\mathbf{q}}|0\rangle_{\mathbf{q}'} + |0\rangle_{\mathbf{p}}|0\rangle_{\mathbf{p}'}|1\rangle_{\mathbf{q}}|1\rangle_{\mathbf{q}'}), \quad (1)$$

where ($\mathbf{p}$,$\mathbf{p}'$) and ($\mathbf{q}$,$\mathbf{q}'$) (illustrated in Fig. 1) correspond to correlated momentum modes in the top (red) and bottom (blue) halos, respectively, satisfying, $\mathbf{p}+\mathbf{p}' = -2\mathbf{k}_0$, $\mathbf{q}+\mathbf{q}' = -4\mathbf{k}_0$, $\mathbf{p} - 2\mathbf{k}_0 = \mathbf{q}$ and $\mathbf{p}' - 2\mathbf{k}_0 = \mathbf{q}'$.

Interferometry and single-atom detection. We wait a separation time of 350 μs ($= t_1$) after the collision pulse (t_0) to apply a series of Bragg pulses - mirror (at t_1) and beamsplitter (at $t_2 = t_1 + 350$ μs) pulses (see Supplementary Methods for details on Bragg pulse characterisation and optimisation) - to selectively couple the momentum modes: ($\mathbf{p}$,$\mathbf{p}'$) and ($\mathbf{q}$,$\mathbf{q}'$), whose total paths through the interferometer are indistinguishable and interfere. The interference is manipulated through phases ϕ_L and ϕ_R imparted onto the momentum modes by the beamsplitter pulse. In our experimental setup, we are limited to equal phase settings $\phi_L = \phi_R$ controlled via the relative phase of a single pair of Bragg laser beams that we use to globally address all momentum modes within the halos. We refer to this setup as a Rarity-Tapster type matter-wave interferometer [17, 23] (Fig. 1c).

To detect atoms, we utilize a micro-channel plate (MCP) and a delay line detector (DLD) system located 848 mm below the trap that provides three-dimensional (3D) resolved detection with single atom resolution [40]. From spatial-temporal information the DLD records, we can reconstruct the velocity (i.e., momentum) distribution of the atoms, enabling us to measure multi-atom momentum correlations within our system [39]. We begin with a raw reconstruction of the 3D momenta of the atoms and then proceed through several post-processing stages, involving coordinate transformations, filtering, and masking, to accurately determine the correlations between selected atomic momenta.

Momentum-correlations and non-local characterisation. Forming the central basis in the analysis of our experiment is the measurement of two-particle momentum correlations between atoms in opposite momentum modes $\mathbf{k}$, $-\mathbf{k}+\Delta\mathbf{k}$ of the scattering halos given by [39],

$$g^{(2)}(\Delta\mathbf{k}) \equiv g^{(2)}(\mathbf{k}, \text{-}\mathbf{k}+\Delta\mathbf{k}) = \frac{\sum_{\mathbf{k}\in V}\langle :\hat{n}_{\mathbf{k}}\hat{n}_{\text{-}\mathbf{k}+\Delta\mathbf{k}}:\rangle}{\sum_{\mathbf{k}\in V}\langle\hat{n}_{\mathbf{k}}\rangle\langle\hat{n}_{\text{-}\mathbf{k}+\Delta\mathbf{k}}\rangle}, \quad (2)$$

where $\hat{n}$ denotes the momentum-mode number operator and V is the volume of the scattering halo occupied in momentum space (Fig. 2a). We describe this correlation function as the measurement of the joint probability of detecting atoms in the momenta $\mathbf{k}$,-$\mathbf{k}$+$\Delta\mathbf{k}$ divided by the product of their individual detection probabilities. Figures 2b and c display the experimentally measured second-order correlation function $g^{(2)}(\Delta k)$ obtained from the pair of scattering halos, where $\Delta k \equiv |\Delta\mathbf{k}|$. The high amplitude observed at $\Delta k = 0$ indicates the generation of highly correlated atom pairs and is set by the mode occupancy $\bar{n}$ (following the relationship, $g^{(2)}(0) = 2+1/\bar{n}$ [39]), which represents the average number density of a scattering mode whose volume is set by the momentum correlation widths of the source condensate [41]. We reach averaged amplitudes of $g^{(2)}(0) \sim 30$ for each of the halos (Fig. 2, b and c) corresponding to average mode occupancies of $\bar{n} \approx 0.035$, demonstrating correlation amplitudes consistent with those required to violate a Bell inequality [19, 42].

In the interferometer, the spatially separated atoms in the entangled momentum modes ($\mathbf{p}$, $\mathbf{p}'$) and ($\mathbf{q}$, $\mathbf{q}'$) must be made to overlap to observe significant multi-particle interference [22]. This interference depends on the phases applied by the beam splitter pulse on each separated arm of the interferometer (Fig. 1c). Successfully achieving this multi-particle interference with independently adjustable phases is essential to effectively demonstrate quantum non-locality in the sense of a violation of the CHSH-Bell inequality [43]. We can observe this multi-particle interference at the output of our interferometer by measuring the joint probability distribution function or population correlations $P_{\mathbf{k},\mathbf{k}'}$ between entangled momentum pairs ($\mathbf{p}$, $\mathbf{p}'$) and ($\mathbf{q}$, $\mathbf{q}'$). This is defined as $P_{\mathbf{k},\mathbf{k}'} = \langle\hat{a}^\dagger_{\mathbf{k}}\hat{a}^\dagger_{\mathbf{k}'}\hat{a}_{\mathbf{k}'}\hat{a}_{\mathbf{k}}\rangle = \langle\hat{n}_{\mathbf{k}}\hat{n}_{\mathbf{k}'}\rangle$ (where $\mathbf{k} \in \{\mathbf{p},\mathbf{q}\}$ and $\mathbf{k}' \in \{\mathbf{p}',\mathbf{q}'\}$) and measures correlations between joint-detection events at the outputs of the left (L) and right (R) arms of the interferometer. Taking the input of our interferometer as the momentum-entangled Bell state in Eq. (1) and treating the mirror and beamsplitter pulses of the interferometer as instantaneous linear transformations (see Supplementary Note 2), we arrive at the joint

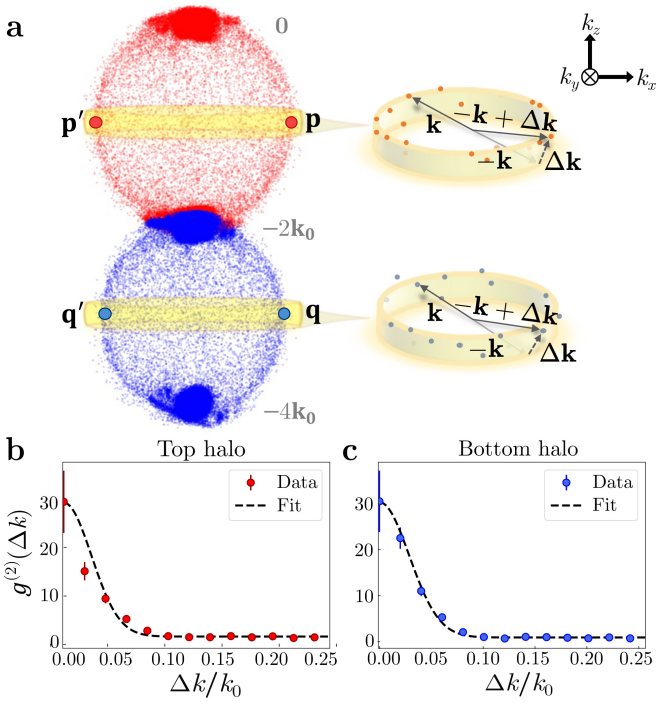

Fig. 2. Two-particle momentum correlations in scattering halos. **a** Experimental data from 1000 shots showing the momentum distribution of the initial double s-wave scattering halo state. The yellow annulus about the equator of each halo depicts the chosen detection window range with a vertical range of $\pm 4^\circ$ about the equator. **b**, **c** Measured $g^{(2)}(\Delta k)$, with $\Delta k \equiv |\Delta\mathbf{k}|$ and $k_0 \equiv |\mathbf{k}_0|$, for the 'Top halo'- between 0 and $-2\mathbf{k}_0$ (red), and the 'Bottom halo'- between $-2\mathbf{k}_0$ and $-4\mathbf{k}_0$ (blue), respectively. Error bars show the shot noise for each data point and solid lines are Gaussian fits to the data.

probability distribution functions

$$P_{\mathbf{p},\mathbf{p}'} = P_{\mathbf{q},\mathbf{q}'} = \frac{1}{2}\sin^2\left(\frac{\phi_L+\phi_R}{2}\right) = \frac{1}{2}\sin^2(\Phi/2) \quad (3)$$

and

$$P_{\mathbf{p},\mathbf{q}'} = P_{\mathbf{q},\mathbf{p}'} = \frac{1}{2}\cos^2\left(\frac{\phi_L+\phi_R}{2}\right) = \frac{1}{2}\cos^2(\Phi/2), \quad (4)$$

with respect to the output state. Interference of the scattered pairs is illustrated by the dependence of the joint probability distribution function on the combined phase $\Phi = \phi_L + \phi_R$, where ϕ_L and ϕ_R represent the beamsplitter phases imparted on the momentum modes $\{\mathbf{p}, \mathbf{q}\}$ and $\{\mathbf{p}', \mathbf{q}'\}$, respectively. Although our experimental configuration only allows for uniform control of the phases, i.e. $\phi_L = \phi_R$, Eqs. (3) and (4) demonstrate that it is still possible to use the global phase $\Phi = \phi_L + \phi_R$ (instead of the relative phase $\phi_L - \phi_R$ as in the original Rarity-Tapster scheme [17, 19]) to demonstrate entanglement and Bell correlations present in the initial state.

Figure 3a displays the experimental joint probability distribution functions measured at the output of the interferometer as we vary the global phase Φ. We observe strong out-of-phase oscillations of the joint probabilities consistent with the predictions of the ideal Bell state (Eqs. (3) and (4)), confirming the existence of multi-particle interference in our setup.

From the joint probability distribution functions, we can obtain the Bell correlation function

$$E(\Phi) = \frac{P_{\mathbf{p},\mathbf{p}'} + P_{\mathbf{q},\mathbf{q}'} - P_{\mathbf{p},\mathbf{q}'} - P_{\mathbf{q},\mathbf{p}'}}{P_{\mathbf{p},\mathbf{p}'} + P_{\mathbf{q},\mathbf{q}'} + P_{\mathbf{p},\mathbf{q}'} + P_{\mathbf{q},\mathbf{p}'}}, \quad (5)$$

which is expected to have the general form [44]

$$E(\Phi) = -A\cos(\Phi' + \delta). \quad (6)$$

Here, $\Phi = \Phi' + \delta$ is the absolute combined phase acquired by the atoms from the beamsplitter pulse, where δ is a phase offset that incorporates any deviation from the experimentally set phase Φ'.

The ideal Bell state (Eq. (1)) would yield an amplitude of $A = 1$, following from Eqs. (3) and (4). However, contributions from higher-order Fock states in the entangled pair generation process lead to a reduced amplitude $A = (1+\bar{n})/(1+3\bar{n})$ expressed in terms of the average mode occupancy $\bar{n}$ [19, 42]. The additional phase offset δ in Eq. (6) accounts for details in the precise implementation of the Rarity-Tapster interferometer, such as path length differences between the two Bragg beams and phase drifts experienced by the scattered particles as they follow free-fall trajectories in a uniform gravitational potential.

The Bell correlation function $E(\Phi)$ constructed from the experimentally detected joint probabilities is shown in Fig. 3b. We find remarkable agreement with both a sinusoidal fit function, consistent with the expectation (Eq. (6)), as well as theory predictions (represented by the black-dotted line) with $A = (1+\bar{n})/(1+3\bar{n})$ computed from the experimentally obtained average mode occupancy.

We further characterise our observed correlations by demonstrating the distinct nonlocal behaviour in our system through a violation of a steering inequality [11, 45–47]. From the steering inequality, we construct (see Supplementary Note 3 for details on the nonlocality criterion) the following nonlocality criterion using the values that $E(\Phi)$ takes at complementary global phase settings,

$$\mathcal{C}(\Phi, \Phi+\pi) = |E(\Phi) - E(\Phi+\pi)| > \sqrt{2}. \quad (7)$$

Satisfying this criterion implies a violation of the steering inequality, $\mathcal{C}(\Phi, \Phi+\pi) \leq \sqrt{2}$, thus demonstrating that a set of correlations observed in our system cannot be described by a wide range of hybrid *local hidden variable* (LHV)—*local hidden state* (LHS) models [45, 46, 48] (see Supplementary Note 3). We plot the LHS of Eq. (7) in Fig. 3c using the experimentally constructed values of $E(\Phi)$ (markers), a sinusoidal fit of $E(\Phi)$ (solid mauve line) and theory predictions (black-dotted line). The strong oscillations in the Bell correlation function lead to an observed maximum violation of $\mathcal{C}(\Phi, \Phi+\pi) =$

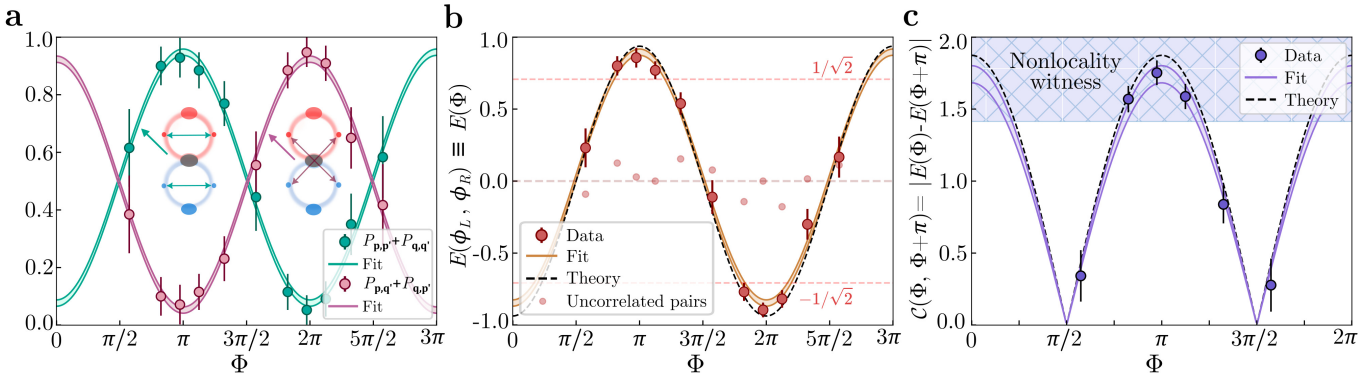

Fig. 3. **Multi-particle interference and non-classical correlations**. Experimental data from over 35,000 shots. **a** Global phase (Φ)-sensitive joint probability distribution function experimentally measured at the interferometer output as Φ is varied. Teal data points represent the measured values of $(P_{\mathbf{p},\mathbf{p}'}+P_{\mathbf{q},\mathbf{q}'})$, while magenta data points correspond to $(P_{\mathbf{q},\mathbf{p}'}+P_{\mathbf{p},\mathbf{q}'})$. **b** The Bell correlation function $E(\Phi)$ with a sinusoidal fit following Eq. (6), where we obtain an amplitude of $A = 0.86(3)$ and phase-offset $\delta = 1.02(4)$. The light-coloured data points around $E = 0$ indicate uncorrelated atom pairs passing through the interferometer, demonstrating expected near-zero Bell correlation amplitudes (see Supplementary Note 3). **c** A nonlocality witness $\mathcal{C}$ constructed from values of the Bell correlation function E at complimentary phase settings. Data points located within the shaded region ($> \sqrt{2}$) indicate the presence of Bell correlations strong enough to exclude a class of LHV theories, with an observed maximum violation of $\sim 3.9\sigma$ at $\mathcal{C}(\Phi, \Phi+\pi) = 1.752 \pm 0.085$ when $\Phi = 3.062$. All error bars correspond to standard deviation estimates using a binomial proportional estimator (see Supplementary Methods for details on the error analysis) with solid lines being fits to the data. The theoretical prediction (black-dashed line) is Eq. (6).

$1.752 \pm 0.085 > \sqrt{2}$ (i.e., a violation of about $\sim 3.9\sigma$) at $\Phi = 3.062$.

DISCUSSION

The violation of the inequality (Eq. (7)) is dependent on the Bell correlation function $E(\Phi)$ displaying a sufficiently large difference between the maximal and minimal correlation, as well as following a particular functional form. In the context of Eq. (6), this reduces to a requirement that the oscillation amplitude exceeds $A > 1/\sqrt{2}$. Such a requirement on A is also shared by more stringent tests of nonlocality, including the celebrated CHSH-Bell inequality [43, 44]. However, in the context of Bell nonlocality an equally important aspect that leads to the incompatibility of quantum mechanics with LHV theories is the sinusoidal variation of the Bell correlation function [2]. In Fig. **3**b we demonstrate that our experimental observations feature both key elements by fitting Eq. (6) to our experiment observations, which yields a fitted value of $A = 0.86(3)$. This signals the detection of Bell correlations in our experiment with the potential to violate the CHSH-Bell inequality upon the implementation of independent phase settings in the spatially separate regions of L and R. This is a major improvement on our previous work [23], where we were unable to demonstrate multi-particle interference sufficient for a non-locality violation. This was possible due to key improvements to the experimental setup that yielded higher correlation amplitudes and signal-to-noise ratio. Such improvements include upgrading the micro-channel plates to have a higher quantum efficiency, frequency-locking the Bragg beams to minimize frequency fluctuations and narrowing the detection windows to only ±4 deg around the equator of the halo (see Methods) for increased precision.

In conclusion, we generate momentum-entangled pairs of massive particles by colliding atomic BECs to form dual s-wave collision halos. Using Bragg beams, we coherently manipulate the momentum states of the scattered atoms, allowing for selective coupling of desired atom pairs in momentum states ($\mathbf{p}$,$\mathbf{p}'$,$\mathbf{q}$,$\mathbf{q}'$) and imparting an arbitrary global phase onto them.

We have observed two-particle correlations dependent on the global interferometric phase Φ and having a sufficiently strong amplitude A that signal the detection of nonclassical, nonlocal Bell correlations in our experiment. This demonstration could be extended by adding independent phase settings in separate regions of the scattering halos to test a CHSH-Bell inequality violation [43] using momentum-entangled states of atoms, an even stronger bound on nonlocality.

We remind the reader that an important aspect in any such future demonstration would be to ensure large space-like separation between the correlated atoms, required for closing the locality loophole. To ensure this, the independent phase setting ϕ_L and ϕ_R must be invoked at a time when the atom pairs are already space-like separated. Given that our detection resolution in time is approximately 1 ns, this requirement implies that the atom pairs must be separated by at least 30 cm. For comparison, the diameter of our current atom detector is 8 cm, which—while being significantly smaller than 30 cm—is not out of reach of the next generation of experiments.

The future development of this scheme could poten-

tially involve generating momentum-entanglement between isotopes of helium—specifically, ^{3}He* and ^{4}He* [49]. This entanglement between momentum states of atoms with different masses would offer a suitable basis for the testing of the weak equivalence principle with quantum test masses [50]. Furthermore, such a platform for entangling massive particles could be useful in examining decoherence theories in quantum systems influenced by gravitational field interactions [12, 51–54], and enhance our understanding of the relation between quantum theory and gravity, as described by general relativity.

Our findings not only establish a new platform for testing the fundamental principles of quantum mechanics but also open avenues for exploring quantum information protocols that leverage motional entanglement [55–57]. Demonstrating and controlling momentum-entanglement in ultracold atomic systems holds promise for advancing quantum technologies such as quantum sensing and quantum imaging through sub-shot noise atom interferometry [58, 59].

METHODS

Condensate formation and atom-optical control. Using a bi-planar quadrupole Ioffe configuration magnetic trap [60], we prepare our ^{4}He* BEC of $\sim 10^5$ atoms in a harmonic potential with frequencies of $(\omega_x, \omega_y, \omega_z)/2\pi \approx (15, 25, 25)$ Hz. The magnetic trap is then rapidly switched off, where we then wait approximately 1.5 ms for the background magnetic field to stabilise to a uniform magnetic field $\mathbf{B}_0 \approx [0.5(\hat{\mathbf{x}}+\hat{\mathbf{z}}) - 0.8\hat{\mathbf{y}}]$ G which is maintained for the remainder of the experiment. The atoms' momentum and internal states are manipulated using resonant two-photon Raman and Bragg transitions, which utilize two orthogonal laser beams aligned along the $(\hat{\mathbf{x}} \pm \hat{\mathbf{z}})/\sqrt{2}$ directions. The beams are frequency-locked and tuned to have optical frequencies far-detuned (to the blue) from the $2^3S_1 \rightarrow 2^3P_0$ transition by 2.3 GHz (Fig. 1, a and b), to minimize single-photon absorption. With these laser beams, a series of light pulses is employed to transfer groups of atoms between different momentum and internal states (see Supplementary Methods for a detailed characterisation of the Bragg pulses).

Detection and scattering halo analysis. Exploiting the ∼19.8 eV internal energy of the metastable helium atoms, we can measure single atom detection events at the microchannel plate (MCP) and delay line detector (DLD) with an estimated quantum efficiency of 20(2)% [61] and spatial-temporal resolutions of 120 μm and 3 μs [62], corresponding to a momentum resolution of about $\sim (4.5 \times 10^{-3})k_0$ along $k_{x,y}$ and $\sim (4.6 \times 10^{-4})k_0$ along k_z.

From the reconstructed velocities of the atoms, we accurately determine the momenta of the scattered atoms by performing coordinate transforms for each of the halos into the centre-of-momentum (COM) reference frame for respective halos. Due to the number of scattered atoms in the halos being relatively few (< 100), we determine the COM of the halo using its colliding parent condensates which have a higher number of atoms ($\sim 3 \times 10^3$). This estimation of the position of the COM is a good approximation of the true COM of the halo. Further, we perform this coordinate transform to the halo COM reference frame for each experimental run, thus minimizing any broadening or skewing of momentum distributions due to shot-to-shot fluctuations when integrating over multiple datasets. We also perform dataset filtering based on the number of scattered atoms in the halos to ensure that we analyse datasets having similar mode occupancy ($\bar{n} \approx 0.035$) and hence consistent two-particle correlation amplitudes $g^{(2)}(0)$.

We obtain the measured correlation results by limiting our detection windows around each of the halo equators. This is to ensure that selected momentum modes within our detection window experience nearly uniform and identical coupling from the Bragg transfer pulses (see Supplementary Methods). Specifically, we only include scattered pairs having radial velocities of $0.8 \leq v/v_r \leq 1.1$ (v_r is the velocity radius of the scattering halo equal to ~ 65 mm/s), and pairs within $\pm 4°$ from the halo's equatorial plane, corresponding to a vertical velocity range of ± 4.5 mm/s about the equator. We arrive at this detection window range as a balance between two competing constraints – minimizing unintentional averaging of the imprinted phases of the scattered pairs across the detection range resulting in decreased interference contrast and reduced joint-detection probabilities at the output of the interferometer, and maximizing the signal-to-noise ratio (SNR) through integrating over a wider scattered momentum range. Our chosen detection window ranges $\{D_{L1}, D_{L2}, D_{R1}, D_{R2}\}$ are shown in Fig. 1c, within which the phase varies by approximately 1.5 radians due to particle-path trajectories, and we achieve an average SNR of 30:1. From this truncated distribution we measure the pair-correlations between the scattered atoms, where we define the size of the integration volume (equivalently, size of a scattering mode) as a cubic volume with sides equal to $\sim 0.02 \times \mathrm{k}_r$ ($\mathrm{k}_r = m \cdot v_r/\hbar$). The side length of integration volume is approximately $0.5\sigma_{BB}$, where σ_{BB} represents the two-atom back-to-back correlation length [39]. This length follows from the relation $\sigma_{BB} \approx 1.1\sigma_k$, with σ_k being the rms momentum width of the source condensate, assuming it can be approximated by an isotropic Gaussian distribution [41]. The small integration volume size also ensures several bins are within the detection window range.

DATA AVAILABILITY

The data that support the findings of this study are available from Zenodo at [63].

REFERENCES

[1] J. S. Bell, *Speakable and Unspeakable in Quantum Mechanics* (Cambridge Univ. Press, Cambridge, 1987).

[2] A. Aspect, Bell's theorem: The naive view of an experimentalist, arXiv:quant-ph/0402001 (2004).

[3] A. Aspect, P. Grangier, and G. Roger, Experimental Tests of Realistic Local Theories via Bell's Theorem, Phys. Rev. Lett. **47**, 460 (1981).

[4] A. Aspect, J. Dalibard, and G. Roger, Experimental Test of Bell's Inequalities Using Time- Varying Analyzers, Phys. Rev. Lett. **49**, 1804 (1982).

[5] M. Giustina, M. A. M. Versteegh, S. Wengerowsky, J. Handsteiner, A. Hochrainer, K. Phelan, F. Steinlechner, J. Kofler, J.-A. Larsson, C. Abellán, W. Amaya, V. Pruneri, M. W. Mitchell, J. Beyer, T. Gerrits, A. E. Lita, L. K. Shalm, S. W. Nam, T. Scheidl, R. Ursin, B. Wittmann, and A. Zeilinger, Significant-loophole-free test of bell's theorem with entangled photons, Phys. Rev. Lett. **115**, 250401 (2015).

[6] L. K. Shalm, E. Meyer-Scott, B. G. Christensen, P. Bierhorst, M. A. Wayne, M. J. Stevens, T. Gerrits, S. Glancy, D. R. Hamel, M. S. Allman, K. J. Coakley, S. D. Dyer, C. Hodge, A. E. Lita, V. B. Verma, C. Lambrocco, E. Tortorici, A. L. Migdall, Y. Zhang, D. R. Kumor, W. H. Farr, F. Marsili, M. D. Shaw, J. A. Stern, C. Abellán, W. Amaya, V. Pruneri, T. Jennewein, M. W. Mitchell, P. G. Kwiat, J. C. Bienfang, R. P. Mirin, E. Knill, and S. W. Nam, Strong loophole-free test of local realism, Phys. Rev. Lett. **115**, 250402 (2015).

[7] M. A. Rowe, D. Kielpinski, V. Meyer, C. A. Sackett, W. M. Itano, C. Monroe, and D. J. Wineland, Experimental violation of a Bell's inequality with efficient detection, Nature **409**, 791 (2001).

[8] B. Hensen, H. Bernien, A. E. Dréau, A. Reiserer, N. Kalb, M. S. Blok, J. Ruitenberg, R. F. L. Vermeulen, R. N. Schouten, C. Abellán, W. Amaya, V. Pruneri, M. W. Mitchell, M. Markham, D. J. Twitchen, D. Elkouss, S. Wehner, T. H. Taminiau, and R. Hanson, Loophole-free Bell inequality violation using electron spins separated by 1.3 kilometres, Nature **526**, 682 (2015).

[9] R. Schmied, J.-D. Bancal, B. Allard, M. Fadel, V. Scarani, P. Treutlein, and N. Sangouard, Bell correlations in a Bose-Einstein condensate, Science **352**, 441 (2016).

[10] L. Pezzè, A. Smerzi, M. K. Oberthaler, R. Schmied, and P. Treutlein, Quantum metrology with nonclassical states of atomic ensembles, Rev. Mod. Phys. **90**, 035005 (2018).

[11] D. K. Shin, B. M. Henson, S. S. Hodgman, T. Wasak, J. Chwedeńczuk, and A. G. Truscott, Bell correlations between spatially separated pairs of atoms, Nat. Commun. **10**, 4447 (2019).

[12] R. Penrose, On Gravity's role in Quantum State Reduction, Gen. Relat. Gravit. **28**, 581 (1996).

[13] A. Khrennikov, The present situation in quantum theory and its merging with general relativity, Found. Phys. **47**, 1077 (2017).

[14] R. Howl, L. Hackermüller, D. E. Bruschi, and I. Fuentes, Gravity in the quantum lab, Adv. Phys. **3**, 1383184 (2018).

[15] R. Howl, R. Penrose, and I. Fuentes, Exploring the unification of quantum theory and general relativity with a Bose–Einstein condensate, New J. Phys. **21**, 043047 (2019).

[16] A. Ashtekar and E. Bianchi, A short review of loop quantum gravity, Rep. Prog. Phys. **84**, 042001 (2021).

[17] J. G. Rarity and P. R. Tapster, Experimental violation of Bell's inequality based on phase and momentum, Phys. Rev. Lett. **64**, 2495 (1990).

[18] W. Vassen, C. Cohen-Tannoudji, M. Leduc, D. Boiron, C. I. Westbrook, A. Truscott, K. Baldwin, G. Birkl, P. Cancio, and M. Trippenbach, Cold and trapped metastable noble gases, Rev. Mod. Phys. **84**, 175 (2012).

[19] R. J. Lewis-Swan and K. V. Kheruntsyan, Proposal for a motional-state Bell inequality test with ultracold atoms, Phys. Rev. A **91**, 052114 (2015).

[20] J. Kofler, M. Singh, M. Ebner, M. Keller, M. Kotyrba, and A. Zeilinger, Einstein-podolsky-rosen correlations from colliding bose-einstein condensates, Phys. Rev. A **86**, 032115 (2012).

[21] M. Keller, M. Kotyrba, F. Leupold, M. Singh, M. Ebner, and A. Zeilinger, Bose-einstein condensate of metastable helium for quantum correlation experiments, Phys. Rev. A **90**, 063607 (2014).

[22] P. Dussarrat, M. Perrier, A. Imanaliev, R. Lopes, A. Aspect, M. Cheneau, D. Boiron, and C. I. Westbrook, Two-Particle Four-Mode Interferometer for Atoms, Phys. Rev. Lett. **119**, 173202 (2017).

[23] K. F. Thomas, B. M. Henson, Y. Wang, R. J. Lewis-Swan, K. V. Kheruntsyan, S. S. Hodgman, and A. G. Truscott, A matter-wave Rarity–Tapster interferometer to demonstrate non-locality, Eur. Phys. J. D **76**, 244 (2022).

[24] C. Leprince, V. Gondret, C. Lamirault, R. Dias, Q. Marolleau, D. Boiron, and C. I. Westbrook, Coherent coupling of momentum states: Selectivity and phase control, Physical Review A **111**, 063304 (2025).

[25] M. Perrier, Z. Amodjee, P. Dussarrat, A. Dareau, A. Aspect, M. Cheneau, D. Boiron, and C. I. Westbrook, Thermal counting statistics in an atomic two-mode squeezed vacuum state, SciPost Phys. **7**, 002 (2019).

[26] A. Perrin, H. Chang, V. Krachmalnicoff, M. Schellekens, D. Boiron, A. Aspect, and C. I. Westbrook, Observation of Atom Pairs in Spontaneous Four-Wave Mixing of Two Colliding Bose-Einstein Condensates, Phys. Rev. Lett. **99**, 150405 (2007).

[27] A. Perrin, C. M. Savage, D. Boiron, V. Krachmalnicoff, C. I. Westbrook, and K. Kheruntsyan, Atomic four-wave mixing via condensate collisions, New J. Phys. **10**, 045021 (2008).

[28] R. I. Khakimov, B. M. Henson, D. K. Shin, S. S. Hodgman, R. G. Dall, K. G. H. Baldwin, and A. G. Truscott, Ghost imaging with atoms, Nature **540**, 100 (2016).

[29] K. Kim, J. Hur, S. Huh, S. Choi, and J.-y. Choi, Emission of spin-correlated matter-wave jets from spinor bose-einstein condensates, Phys. Rev. Lett. **127**, 043401 (2021).

[30] K. M. Hilligsøe and K. Mølmer, Phase-matched four wave mixing and quantum beam splitting of matter waves in a periodic potential, Phys. Rev. A **71**, 041602 (2005).

[31] G. K. Campbell, J. Mun, M. Boyd, E. W. Streed, W. Ketterle, and D. E. Pritchard, Parametric amplification of scattered atom pairs, Phys. Rev. Lett. **96**, 020406 (2006).

[32] R. Bücker, J. Grond, S. Manz, T. Berrada, T. Betz, C. Koller, U. Hohenester, T. Schumm, A. Perrin, and J. Schmiedmayer, Twin-atom beams, Nat. Phys. **7**, 608 (2011).

[33] M. Bonneau, J. Ruaudel, R. Lopes, J.-C. Jaskula, A. Aspect, D. Boiron, and C. I. Westbrook, Tunable source of correlated atom beams, Phys. Rev. A **87**, 061603 (2013).
[34] R. Lopes, A. Imanaliev, A. Aspect, M. Cheneau, D. Boiron, and C. I. Westbrook, Atomic hong–ou–mandel experiment, Nature **520**, 66 (2015).
[35] F. Finger, R. Rosa-Medina, N. Reiter, P. Christodoulou, T. Donner, and T. Esslinger, Spin- and momentum-correlated atom pairs mediated by photon exchange and seeded by vacuum fluctuations, Phys. Rev. Lett. **132**, 093402 (2024).
[36] S. S. Hodgman, R. G. Dall, L. J. Byron, K. G. H. Baldwin, S. J. Buckman, and A. G. Truscott, Metastable Helium: A New Determination of the Longest Atomic Excited-State Lifetime, Phys. Rev. Lett. **103**, 053002 (2009).
[37] S. Gupta, A. E. Leanhardt, A. D. Cronin, and D. E. Pritchard, Coherent manipulation of atoms with standing light waves, Comptes Rendus de l'Académie des Sciences - Series IV - Physics **2**, 479 (2001).
[38] C. Couteau, Spontaneous parametric down-conversion, Contemp. Phys. **59**, 291 (2018).
[39] S. S. Hodgman, R. I. Khakimov, R. J. Lewis-Swan, A. G. Truscott, and K. V. Kheruntsyan, Solving the Quantum Many-Body Problem via Correlations Measured with a Momentum Microscope, Phys. Rev. Lett. **118**, 240402 (2017).
[40] A. G. Manning, S. S. Hodgman, R. G. Dall, M. T. Johnsson, and A. G. Truscott, The Hanbury Brown-Twiss effect in a pulsed atom laser, Opt. Express **18**, 18712 (2010).
[41] M. Ögren and K. V. Kheruntsyan, Atom-atom correlations in colliding Bose-Einstein condensates, Phys. Rev. A **79**, 021606 (2009).
[42] T. Wasak and J. Chwedeńczuk, Bell Inequality, Einstein-Podolsky-Rosen Steering, and Quantum Metrology with Spinor Bose-Einstein Condensates, Phys. Rev. Lett. **120**, 140406 (2018).
[43] J. F. Clauser, M. A. Horne, A. Shimony, and R. A. Holt, Proposed Experiment to Test Local Hidden-Variable Theories, Phys. Rev. Lett. **23**, 880 (1969).
[44] J. F. Clauser and A. Shimony, Bell's theorem. Experimental tests and implications, Rep. Prog. Phys. **41**, 1881 (1978).
[45] H. M. Wiseman, S. J. Jones, and A. C. Doherty, Steering, Entanglement, Nonlocality, and the Einstein-Podolsky-Rosen Paradox, Phys. Rev. Lett. **98**, 140402 (2007).
[46] E. G. Cavalcanti, S. J. Jones, H. M. Wiseman, and M. D. Reid, Experimental criteria for steering and the Einstein-Podolsky-Rosen paradox, Phys. Rev. A **80**, 032112 (2009).
[47] S. J. Jones, H. M. Wiseman, and A. C. Doherty, Entanglement, Einstein-Podolsky-Rosen correlations, Bell nonlocality, and steering, Phys. Rev. A **76**, 052116 (2007).
[48] E. G. Cavalcanti, C. J. Foster, M. Fuwa, and H. M. Wiseman, Analog of the Clauser–Horne–Shimony–Holt inequality for steering, J. Opt. Soc. Am. B **32**, A74 (2015).
[49] X. T. Yan, S. Kannan, Y. S. Athreya, A. G. Truscott, and S. S. Hodgman, Proposal for a Bell Test with Entangled Atoms of Different Mass, Quantum **9**, 1939 (2025).
[50] R. Geiger and M. Trupke, Proposal for a Quantum Test of the Weak Equivalence Principle with Entangled Atomic Species, Phys. Rev. Lett. **120**, 043602 (2018).
[51] E. Alvarez, Quantum gravity: An introduction to some recent results, Rev. Mod. Phys. **61**, 561 (1989).
[52] M. Zych, F. Costa, I. Pikovski, and Č. Brukner, Quantum interferometric visibility as a witness of general relativistic proper time, Nat. Commun. **2**, 505 (2011).
[53] S. Vowe, S. Donadi, V. Schkolnik, A. Peters, B. Leykauf, and M. Krutzik, Light-pulse atom interferometric test of continuous spontaneous localization, Phys. Rev. A **106**, 043317 (2022).
[54] G. Ciliberto, S. Emig, N. Pavloff, and M. Isoard, Violation of bell inequalities in an analog black hole, Phys. Rev. A **109**, 063325 (2024).
[55] S. L. Braunstein and P. van Loock, Quantum information with continuous variables, Rev. Mod. Phys. **77**, 513 (2005).
[56] M. N. O'Sullivan-Hale, I. Ali Khan, R. W. Boyd, and J. C. Howell, Pixel entanglement: Experimental realization of optically entangled $d = 3$ and $d = 6$ qudits, Phys. Rev. Lett. **94**, 220501 (2005).
[57] S. P. Walborn, D. S. Lemelle, M. P. Almeida, and P. H. S. Ribeiro, Quantum key distribution with higher-order alphabets using spatially encoded qudits, Phys. Rev. Lett. **96**, 090501 (2006).
[58] F. Anders, A. Idel, P. Feldmann, D. Bondarenko, S. Loriani, K. Lange, J. Peise, M. Gersemann, B. Meyer-Hoppe, S. Abend, N. Gaaloul, C. Schubert, D. Schlippert, L. Santos, E. Rasel, and C. Klempt, Momentum Entanglement for Atom Interferometry, Phys. Rev. Lett. **127**, 140402 (2021).
[59] M. Fadel, N. Roux, and M. Gessner, Quantum metrology with a continuous-variable system, Rep. Prog. Phys. **88**, 106001 (2025).
[60] R. G. Dall and A. G. Truscott, Bose–Einstein condensation of metastable helium in a bi-planar quadrupole Ioffe configuration trap, Opt. Commun. **270**, 255 (2007).
[61] S. Kannan, Y. S. Athreya, A. H. Abbas, X. T. Yan, S. S. Hodgman, and A. G. Truscott, Measurement of the s -wave scattering length between metastable helium isotopes, Phys. Rev. A **110**, 063324 (2024).
[62] B. M. Henson, X. Yue, S. S. Hodgman, D. K. Shin, L. A. Smirnov, E. A. Ostrovskaya, X. W. Guan, and A. G. Truscott, Bogoliubov-Cherenkov radiation in an atom laser, Phys. Rev. A **97**, 063601 (2018).
[63] Research data available from Zenodo at https://doi.org/10.5281/zenodo.17939482.

ACKNOWLEDGEMENTS

The authors would like to thank K.F. Thomas for technical assistance with the early stages of the experiment, and S.A. Haine for helpful discussions. This work was supported through the Australian Research Council (ARC) Discovery Projects, Grant No. DP190103021, DP240101346, DP240101441 and DP240101033. S.S.H. was supported by the Australian Research Council Future Fellowship Grant No. FT220100670. S.K. was supported by an Australian Government Research Training Program scholarship.

AUTHOR CONTRIBUTIONS

Y.S.A. and S.K. performed the experiment and collected the data under the supervision of A.G.T. and S.S.H. All authors contributed to the design of the experiment, the conceptual formulation of the physics and the interpretation of the data. Y.S.A., R.J.L.-S., K.V.K. and S.S.H. wrote the manuscript with input from all authors.

COMPETING INTERESTS

The authors declare no competing interests.

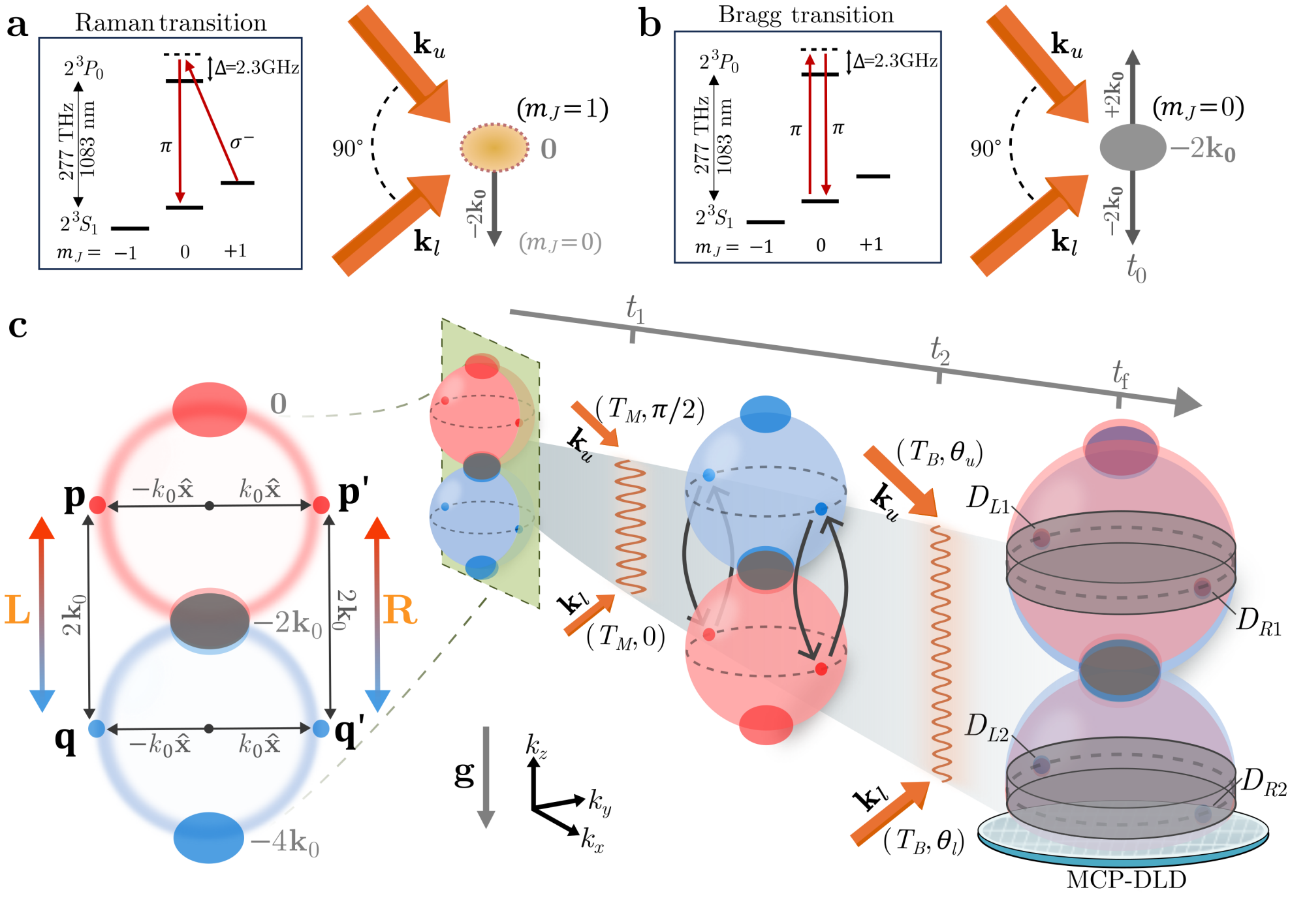
a
Raman transition
2^3P_0
277 THz
1083 nm
2^3S_1
$m_J=$ −1 0 +1
Δ=2.3GHz
π
σ^-
$\mathbf{k}_u$
$\mathbf{k}_l$
90°
$(m_J=1)$
0
$-2\mathbf{k}_0$
$(m_J=0)$
b
Bragg transition
2^3P_0
277 THz
1083 nm
2^3S_1
$m_J=$ −1 0 +1
Δ=2.3GHz
π
π
$\mathbf{k}_u$
$\mathbf{k}_l$
90°
$+2\mathbf{k}_0$
$(m_J=0)$
$-2\mathbf{k}_0$
$-2\mathbf{k}_0$
t_0
c
t_1
t_2
t_f
0
p
p'
q
q'
$-k_0\hat{\mathbf{x}}$
$k_0\hat{\mathbf{x}}$
$2\mathbf{k}_0$
$-2\mathbf{k}_0$
$2\mathbf{k}_0$
$-4\mathbf{k}_0$
L
R
$(T_M, \pi/2)$
$\mathbf{k}_u$
$\mathbf{k}_l$
$(T_M, 0)$
(T_B, θ_u)
$\mathbf{k}_u$
$\mathbf{k}_l$
(T_B, θ_l)
D_{L1}
D_{R1}
D_{L2}
D_{R2}
MCP-DLD
g
k_z
k_y
k_x

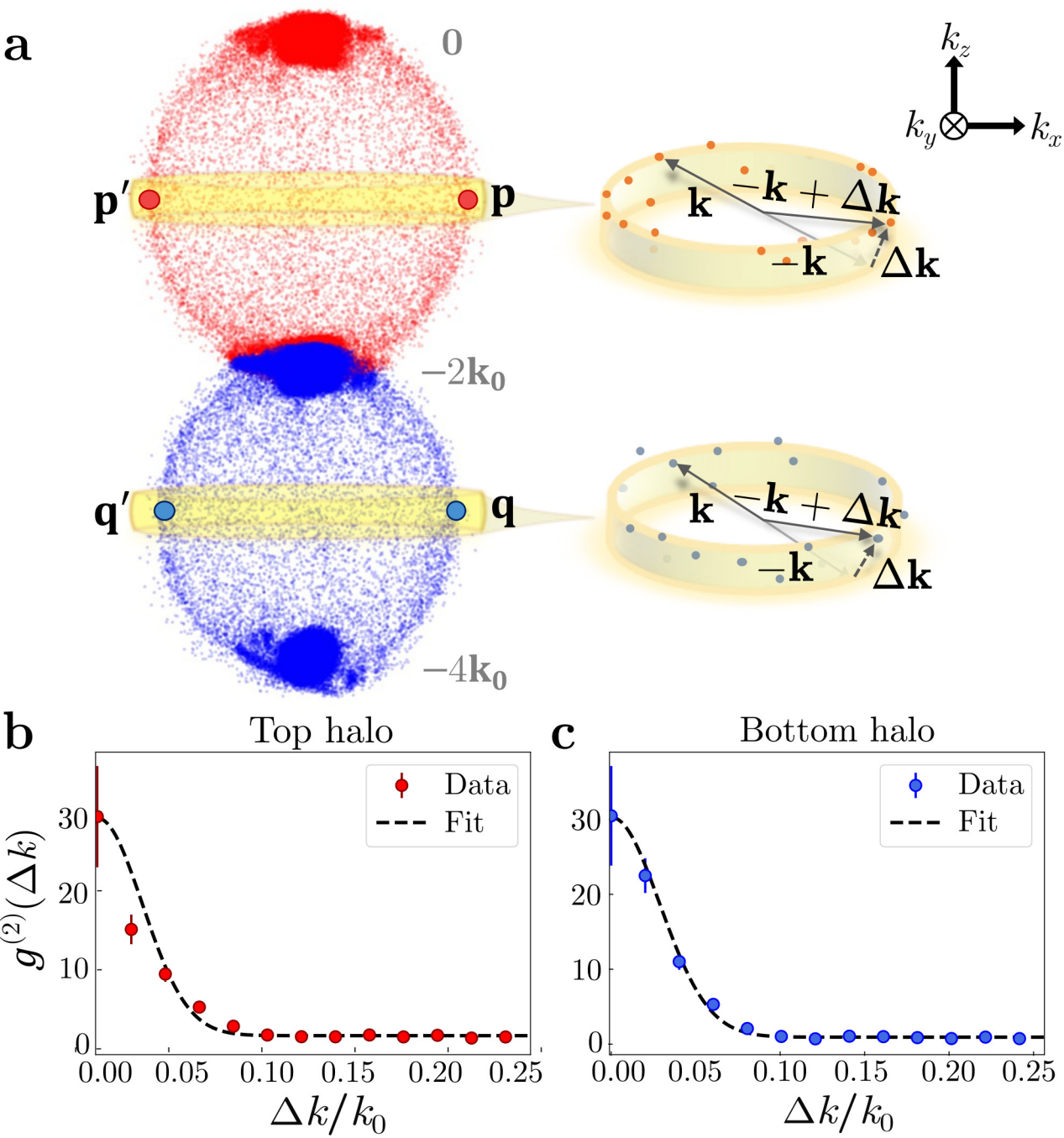
a
0
$-2\mathbf{k_0}$
$-4\mathbf{k_0}$
$\mathbf{p}'$
$\mathbf{p}$
$\mathbf{q}'$
$\mathbf{q}$
k_z
k_y
k_x
$\mathbf{k}$
$-\mathbf{k}+\Delta\mathbf{k}$
$-\mathbf{k}$
$\Delta\mathbf{k}$
b
Top halo
Data
Fit
$g^{(2)}(\Delta k)$
$\Delta k/k_0$
c
Bottom halo
Data
Fit
$\Delta k/k_0$

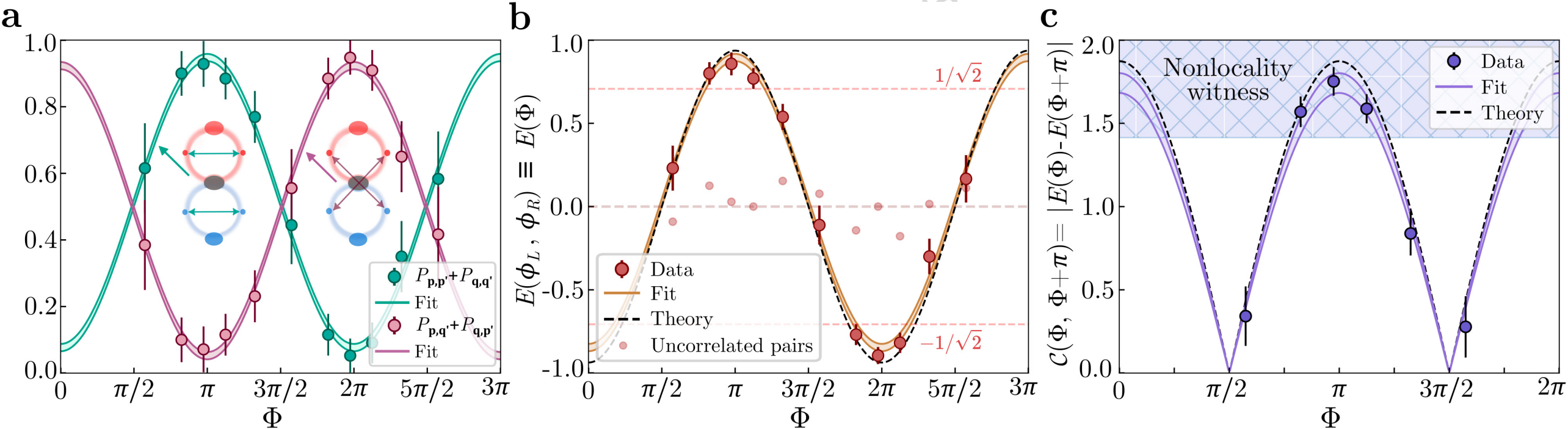
a
1.0
0.8
0.6
0.4
0.2
0.0
0
π/2
π
3π/2
2π
5π/2
3π
Φ
$P_{p,p'}+P_{q,q'}$
Fit
$P_{p,q'}+P_{q,p'}$
Fit
b
$E(\phi_L, \phi_R) \equiv E(\Phi)$
1.0
0.5
0.0
-0.5
-1.0
$1/\sqrt{2}$
$-1/\sqrt{2}$
Data
Fit
Theory
Uncorrelated pairs
c
$\mathcal{C}(\Phi, \Phi+\pi) = |E(\Phi)-E(\Phi+\pi)|$
2.0
1.5
1.0
0.5
0.0
Nonlocality witness
Data
Fit
Theory